Atmos. Chem. Phys., 12, 8851–8864, 2012
www.atmos-chem-phys.net/12/8851/2012/
doi:10.5194/acp-12-8851-2012


Atmospheric Chemistry and Physics

# Analysis of stratospheric $NO_2$ trends above Jungfraujoch using ground-based UV-visible, FTIR, and satellite nadir observations

**F. Hendrick[1], E. Mahieu[2], G. E. Bodeker[3], K. F. Boersma[4,5], M. P. Chipperfield[6], M. De Mazière[1], I. De Smedt[1], P. Demoulin[2], C. Fayt[1], C. Hermans[1], K. Kreher[7], B. Lejeune[2], G. Pinardi[1], C. Servais[2], R. Stübi[8], R. van der A[4], J.-P. Vernier[9,10], and M. Van Roozendael[1]**

[1]Belgian Institute for Space Aeronomy (BIRA-IASB), Brussels, Belgium
[2]Institute of Astrophysics and Geophysics of the University of Liège, Liège, Belgium
[3]Bodeker Scientific, Alexandra, New Zealand
[4]Royal Netherlands Meteorological Institute (KNMI), De Bilt, The Netherlands
[5]Eindhoven University of Technology, Eindhoven, The Netherlands
[6]School of Earth and Environment, University of Leeds, Leeds, UK
[7]National Institute of Water and Atmospheric Research, Omakau, Central Otago, New Zealand
[8]MeteoSwiss, Payerne, Switzerland
[9]Science Systems and Applications, Inc., Hampton, Virginia, USA
[10]NASA Langley Research Center, Hampton, Virginia, USA

*Correspondence to:* F. Hendrick (franch@oma.be)

Received: 15 March 2012 – Published in Atmos. Chem. Phys. Discuss.: 15 May 2012
Revised: 29 August 2012 – Accepted: 11 September 2012 – Published: 28 September 2012

**Abstract.** The trend in stratospheric $NO_2$ column at the NDACC (Network for the Detection of Atmospheric Composition Change) station of Jungfraujoch (46.5° N, 8.0° E) is assessed using ground-based FTIR and zenith-scattered visible sunlight SAOZ measurements over the period 1990 to 2009 as well as a composite satellite nadir data set constructed from ERS-2/GOME, ENVISAT/SCIAMACHY, and METOP-A/GOME-2 observations over the 1996–2009 period. To calculate the trends, a linear least squares regression model including explanatory variables for a linear trend, the mean annual cycle, the quasi-biennial oscillation (QBO), solar activity, and stratospheric aerosol loading is used. For the 1990–2009 period, statistically indistinguishable trends of $-3.7 \pm 1.1\,\%\,\mathrm{decade}^{-1}$ and $-3.6 \pm 0.9\,\%\,\mathrm{decade}^{-1}$ are derived for the SAOZ and FTIR $NO_2$ column time series, respectively. SAOZ, FTIR, and satellite nadir data sets show a similar decrease over the 1996–2009 period, with trends of $-2.4 \pm 1.1\,\%\,\mathrm{decade}^{-1}$, $-4.3 \pm 1.4\,\%\,\mathrm{decade}^{-1}$, and $-3.6 \pm 2.2\,\%\,\mathrm{decade}^{-1}$, respectively. The fact that these declines are opposite in sign to the globally observed $+2.5\,\%\,\mathrm{decade}^{-1}$ trend in $N_2O$, suggests that factors other than $N_2O$ are driving the evolution of stratospheric $NO_2$ at northern mid-latitudes. Possible causes of the decrease in stratospheric $NO_2$ columns have been investigated. The most likely cause is a change in the $NO_2$/NO partitioning in favor of NO, due to a possible stratospheric cooling and a decrease in stratospheric chlorine content, the latter being further confirmed by the negative trend in the $ClONO_2$ column derived from FTIR observations at Jungfraujoch. Decreasing ClO concentrations slows the $NO + ClO \rightarrow NO_2 + Cl$ reaction and a stratospheric cooling slows the $NO + O_3 \rightarrow NO_2 + O_2$ reaction, leaving more $NO_x$ in the form of NO. The slightly positive trends in ozone estimated from ground- and satellite-based data sets are also consistent with the decrease of $NO_2$ through the $NO_2 + O_3 \rightarrow NO_3 + O_2$ reaction. Finally, we cannot rule out the possibility that a strengthening of the Dobson-Brewer circulation, which reduces the time available for $N_2O$ photolysis in the stratosphere, could also contribute to the observed decline in stratospheric $NO_2$ above Jungfraujoch.

**Published by Copernicus Publications on behalf of the European Geosciences Union.**

## 1 Introduction

Nitrogen dioxide ($NO_2$) plays an important role in controlling ozone abundances in the stratosphere (Solomon, 1999), either by destroying ozone through the $NO_x$ ($NO + NO_2$) catalytic destruction cycles, or by mitigating ozone destruction by converting active chlorine, hydrogen, and bromine into their reservoir forms ($ClONO_2$, $HNO_3$, and $BrONO_2$, respectively). The primary source of $NO_x$ is the oxidation of nitrous oxide ($N_2O$) in the middle stratosphere. $N_2O$ is an important greenhouse gas and its emissions in the troposphere are known to be increasing by 2.5–3 % per decade (Liley et al., 2000), mainly due to agricultural activity. Monitoring long-term changes in stratospheric $NO_2$ is essential for attributing observed changes in stratospheric ozone. However, few studies of the long-term evolution of stratospheric $NO_2$ have been published to date. Liley et al. (2000) reported an increase in stratospheric $NO_2$ of about 5 % decade$^{-1}$ from ground-based zenith-scattered visible sunlight measurements at Lauder, New Zealand (45° S, 170° E) between 1981 and 1999. Recently, Dirksen et al. (2011) further confirmed an increase of $NO_2$ of 5 % decade$^{-1}$ over this station for the 1981–2010 period also from ground-based UV-visible data. Using 3-D-Chemical Transport Model calculations, McLinden et al. (2001) suggested that the 5 % decade$^{-1}$ $NO_2$ trend from 1981 to 1999 results from a 2.5 % decade$^{-1}$ increase due to rising $N_2O$ emissions and further 2.5 % decade$^{-1}$ increase resulting from a decrease in stratospheric ozone. The abundance of $NO_2$ in the stratosphere can be affected by ozone through the following reaction (Fish et al., 2000):

$$NO_2 + O_3 \rightarrow NO_3 + O_2 \quad \text{(R1)}$$

Gruzdev (2009) investigated the latitudinal structure of the stratospheric $NO_2$ trend using ground-based zenith-sky UV-visible and FTIR observations from a selection of 23 sites within the Network for the Detection of Atmospheric Composition Change (NDACC). This study, performed over different time periods between 1983 and 2007, showed that the $NO_2$ trend is predominantly positive at mid-latitudes in the Southern Hemisphere while negative trends are observed at most Northern Hemisphere mid-latitude sites. Cook and Roscoe (2009) inferred trends in stratospheric $NO_2$ from measurements obtained during the 1990–2007 period from a zenith-sky UV-visible spectrometer in the Antarctic. The $NO_2$ trend strongly depends on the period, with a positive trend of $\sim$10 % decade$^{-1}$ from 1990 to 2000, a negative trend of $\sim$20 % decade$^{-1}$ from 2000 to 2007, and no overall trend for the full time period. These studies show that the trend in stratospheric $NO_2$ has a complicated structure which does not always follow the evolution of its main source ($N_2O$) and displays a strong dependence on the location and time period considered for the trend analysis.

Trends in stratospheric $NO_2$ at the Jungfraujoch NDACC station in the Swiss Alps (46.5° N, 8.0° E) are quantified and interpreted below. Ground-based UV-visible SAOZ (Système d'Analyse par Observation Zénithale) and Fourier Transform Infra-Red (FTIR) spectrometers have been operating continuously at this station since 1990 and 1985, respectively, providing more than two decades of measurements. A combination of stratospheric $NO_2$ columns retrieved from the ERS-2/GOME (1996–2003), ENVISAT/SCIAMACHY (2003–2009), and METOP-A/ GOME-2 (2007–2009) satellite nadir instruments is also included in this study, permitting, for the first time, a thorough analysis of the long-term evolution of stratospheric $NO_2$ from three (two ground-based and one satellite) independent measurement techniques at this site. The paper is divided into 4 sections. Section 2 provides a description of the ground-based and satellite data sets. The consistency between the different data sets is investigated in Sect. 3 through comparisons between (1) ground-based FTIR and UV-visible $NO_2$ column time series, and (2) satellite and ground-based UV-visible observations. In Sect. 4, the linear least squares regression model used for the trend study is described and the results of the trend analyses are presented and discussed. Conclusions are given in Sect. 5.

## 2 Data sets

### 2.1 SAOZ observations

The SAOZ instrument is a broad-band (300–600 nm), medium resolution ($\sim$1 nm) diode-array spectrometer that measures zenith scattered sunlight (Pommereau and Goutail, 1988). Between 1990 and 2009 two different versions of the SAOZ instrument were used. The first (NMOS) described in Van Roozendael et al. (1994) is based on a Jobin-Yvon spectrometer (model CP200) coupled to a 512 diode Hamamatsu NMOS detector. In December 1998, the system was upgraded to a 1024 diode Hamamatsu detector. This second version (SAM) provides low sun spectra with a better resolution and a higher signal to noise ratio than the NMOS version.

Zenith radiance spectra are analyzed using the DOAS (Differential Optical Absorption Spectroscopy) technique (Platt and Stutz, 2008). $NO_2$ is retrieved in the 425–490 nm wavelength range, taking into account the spectral signatures of $NO_2$, $O_3$, $H_2O$, $O_4$, and the filling-in of the solar Fraunhofer bands by the Ring effect (Grainger and Ring, 1962). The $NO_2$ absorption cross-sections at 220 K are from Vandaele et al. (1998). A third-order polynomial is used to fit the low frequency spectral structure due to molecular and Mie scattering.

$NO_2$ vertical column densities are derived from vertical profiles retrieved by applying a profiling technique to sunrise and sunset $NO_2$ differential slant column densities (DSCDs) which are the direct product of the DOAS analysis. The profiling algorithm is based on the Optimal Estimation Method (OEM; Rodgers, 2000) and is described in Hendrick

et al. (2004). In brief, a profile $\widehat{\mathbf{x}}$ is retrieved given an a priori profile $\mathbf{x}_a$, the measurements $\mathbf{y}$ (here, twilight $NO_2$ DSCDs as a function of solar zenith angle (SZA)), their respective uncertainty covariance matrices ($\mathbf{S}_a$ and $\mathbf{S}_\varepsilon$), and the matrix $\mathbf{K}$ of the weighting functions. Since $NO_2$ is an optically thin absorber, the OEM for the linear case can be considered:

$$\widehat{\mathbf{x}} = \mathbf{x}_a + \mathbf{S}_a\mathbf{K}^T(\mathbf{K}\mathbf{S}_a\mathbf{K}^T + \mathbf{S}_\varepsilon)^{-1}(\mathbf{y} - \mathbf{K}\,\mathbf{x}_a) \quad (1)$$

with $\mathbf{K} = \frac{\partial \mathbf{y}}{\partial \mathbf{x}}$ and $\mathbf{K}^T$ is the transpose of $\mathbf{K}$.

The weighting functions indicate the sensitivity of the measurements to a change in the vertical profile. The matrix $\mathbf{K}$ is determined by consecutively perturbing each layer of the a priori profile and recalculating the set of measurements using the so-called forward model which describes the physics of the measurements. Here, the forward model consists of the stacked photochemical box model PSCBOX coupled to the radiative transfer model (RTM) UVSPEC/DISORT (see Hendrick et al., 2004, 2006 for further details about both models). The photochemical model, initialized daily with chemical and meteorological fields from the SLIMCAT 3-D-CTM (Chipperfield et al., 2006), is able to simulate the rapid variation of $NO_2$ at twilight. The model also provides a priori profiles to the profiling algorithm and is used to photochemically convert the retrieved profiles, which are representative of twilight conditions, to the mean SZA corresponding to the FTIR and satellite nadir observations. The DSCDs are analyzed using daily reference spectra and the effective residual amounts of $NO_2$ in the reference spectra are directly fitted by the profiling algorithm. Combining this with an a priori tropospheric $NO_2$ content close to zero leads to retrieved vertical profiles and corresponding vertical columns mainly representative of the stratosphere (Hendrick et al., 2004, 2008). Performing the DOAS analysis with daily reference spectra also minimizes the potential impact of any long-term degradation of the instrument on the $NO_2$ vertical column time series, which is important for calculating robust trends. $NO_2$ profile retrievals are quality-checked based on the retrieval fit residual (RMS of the difference between measured SCDs and those calculated using the retrieved profiles; see Hendrick et al., 2004). In practice, all retrievals with a residual larger than $3.5 \times 10^{15}$ molec cm$^{-2}$ are rejected. This method of selection excludes measurements contaminated by tropospheric $NO_2$ which usually display short-term variability inconsistent with the expected smooth variation of the stratospheric slant column during twilight. A detailed error budget can be found in Hendrick et al. (2004). Taking into account the smoothing error, the retrieval noise, and the forward model parameter error, the total relative uncertainty on the retrieved stratospheric $NO_2$ columns is about 8 % on average. High aerosol loading can also perturb UV-visible measurements by modifying the scattering geometry. During the period considered in this study (1990–2009), the Mount Pinatubo eruption in June 1991 injected large amounts of aerosols into the stratosphere. In the years immediately following this event (1991–1994), an extinction profile corresponding to a volcanic aerosol loading was selected from the aerosol model of Shettle (1989) and included in the UVSPEC/DISORT RTM for the calculation of the weighting functions needed for the OEM-based profile retrieval. Before and after the 1991–1994 period, a background aerosol extinction profile was used. Sensitivity tests have shown that the use of an aerosol extinction profile corresponding to volcanic conditions has an impact of up to 10 % on the retrieved stratospheric $NO_2$ columns. Aerosol loading changes due to the Mount Pinatubo eruption are also implemented in the SLIMCAT model through the use of monthly zonal mean time series of surface sulfate area density created from different satellite data sets (more details are available at http://homepages.see.leeds.ac.uk/~lecmc/sparc/Forcings/SPARC_Forcings_WMO2011.html).

We have also estimated the impact on the SAOZ columns of using the $NO_2$ cross-sections at 220 K only instead of taking into account the variation of the $NO_2$ cross-sections with the stratospheric temperature. Sensitivity tests in the 425–490 nm range using the Vandaele et al. (1998) $NO_2$ cross-sections at 220 and 294 K show an increase of the $NO_2$ slant column density of 20 % from 220 to 294 K, i.e. an increase of 0.3 %/ K assuming a linear temperature dependence. The $NO_2$ effective temperature, defined as the mean temperature of the stratosphere weighted by the $NO_2$ concentration profile (Gil et al., 2008), is calculated using the temperature and $NO_2$ vertical profiles from the SLIMCAT/PSCBOX model. At Jungfraujoch, it ranges on average from 212 K in winter to 232 K in summer. This means that the correction for the difference between 220 K and the $NO_2$ effective temperature to be applied to the SAOZ $NO_2$ columns is of $-2.4$ % in winter and +3.6 % in summer. On average over the year, we can therefore expect slightly larger SAOZ $NO_2$ columns when applying a correction for the variation of the stratospheric temperature. Consequently, the temperature dependence of the $NO_2$ cross-sections cannot explain the negative trends inferred from this data set (see Sect. 4.2).

### 2.2 Ground-based FTIR observations

In the early 1950s, M. Migeotte performed pioneering atmospheric infrared observations at the Jungfraujoch. Since then, the University of Liège has operated state-of-the-art instruments at that site to record high-resolution spectra allowing production of atlases of the solar spectrum and monitoring of the state of the Earth's atmosphere (Zander et al., 2008 and references therein). This long-term commitment has allowed the collection of a unique observational data base in terms of quality, time extension and measurement density. FTIR high-resolution solar absorption spectra have been recorded regularly under clear-sky conditions since 1985 with a homemade instrument, backed-up in the early 1990s by a commercial

Bruker IFS-120HR. Over the time period of interest here, spectra were obtained on average on 115 days per year.

For this study, all available observations since 1990 have been fitted with the V3.91 of the SFIT-2 algorithm, using pressure and temperature information provided by the National Centers for Environmental Prediction (NCEP, see http://www.ncep.noaa.gov) and assuming the HITRAN 2004 spectroscopic line parameter compilation, including the August 2006 updates (Rothmann et al., 2004, see also http://www.cfa.harvard.edu/hitran). The SFIT-2 code also implements the OEM (Rodgers, 2000), enabling the derivation of the vertical distributions of most of the FTIR target gases (e.g., Pougatchev and Rinsland, 1995; Rinsland et al., 2003a). In the present case, two microwindows ranging from 2914.6 to 2914.7 $cm^{-1}$ and from 2915 to 2915.11 $cm^{-1}$ have been fitted; a priori vertical profiles for fitted ($H_2O$, $CH_4$ and $O_3$ scaled during the retrieval process) and simulated interferences (e.g. $H_2CO$) were based on predictions obtained with the version 5 of the WACCM model (Whole-Atmosphere Community Climate Model, see Chang et al., 2008). For $NO_2$, we used 12 monthly profiles based on the same PSCBOX/SLIMCAT modeled a priori profile data set as for the SAOZ profile retrieval (see Sect. 2.1). The forward model was characterized by a diagonal covariance of 40 % per km and, with extra-diagonal elements based on a Gaussian half-width for interlayer correlation of 4 km. Regarding the error budget, estimates reported in Table 2 of Rinsland et al. (2003a) remain valid (total random and systematic errors of 11 % and 36 %, respectively), although they can be considered as conservative.

### 2.3 Satellite nadir observations

GOME, SCIAMACHY, and GOME-2 stratospheric $NO_2$ columns are retrieved using the KNMI/BIRA TEMIS $NO_2$ algorithm (Boersma et al., 2004, 2007; Dirksen et al., 2011). For this study, we use versions TM4NO2A v1.04 for GOME and TM4NO2A v1.10 for SCIAMACHY and GOME-2, and the periods covered by the different instruments are 1995–2003, 2002–2009, and 2007–2009, respectively. The TEMIS algorithm is based on a two-step process including (1) the retrieval of $NO_2$ slant columns with the DOAS method, and (2) the estimation of the stratospheric component of the $NO_2$ slant columns through data assimilation in the TM4 chemistry transport model. The purpose of the assimilation is to regularly update the TM4 simulation with available measurements such that the model simulation of the stratospheric $NO_2$ column is closely constrained by the satellite measurements. In step 1, the DOAS analysis is performed in the following wavelength ranges: 425–450 nm for GOME and GOME-2 and 426.5–451.5 nm for SCIAMACHY. Absorption by $NO_2$, ozone, water vapor, the Ring effect, and a third-order polynomial that describes the residual broadband features due to Rayleigh and Mie scattering are taken into account. The $NO_2$ cross-sections set at 220 K from Vandaele et al. (1998) is used. A correction for the difference between 220 K and the effective temperature of $NO_2$ along the light path is applied to the $NO_2$ absorption cross-sections. The stratospheric $NO_2$ vertical columns are calculated by dividing the assimilated stratospheric slant columns by a simple geometrical airmass factor depending only on the SZA and viewing angle (Boersma et al., 2004). The estimated error on TEMIS stratospheric $NO_2$ columns is about 0.2–$0.3 \times 10^{15}$ molec $cm^{-2}$ (Boersma et al., 2004; Dirksen et al., 2011).

For this study, all pixels falling within a radius of 300 km around Jungfraujoch were selected and no filtering based on the cloud fraction was applied.

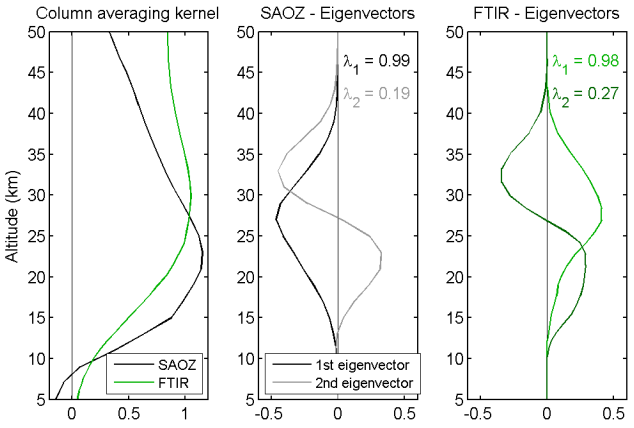


**Fig. 1.** Typical FTIR and SAOZ column averaging kernels (left plot) and leading eigenvectors and corresponding eigenvalues (middle plot: SAOZ; right plot: FTIR). The sum of the latter gives the DOFS.

## 3 Evaluation of data consistency

### 3.1 FTIR and SAOZ data sets comparison

First, we have compared the information content associated with both FTIR and SAOZ profile retrievals. As can be seen in Fig. 1, column averaging kernels are very similar for both techniques with no sensitivity to $NO_2$ in the troposphere and a maximum sensitivity between 20 and 35 km altitude where the $NO_2$ concentration in the stratosphere is the largest. Figure 1 also presents the eigenvector expansion of the averaging kernel matrix **A** corresponding to the two largest eigenvalues. The first eigenvalue, close to unity, implies an almost 100 % contribution of the measurements in this pattern (Hendrick et al., 2004). This pattern also indicates that the altitude range with high sensitivity to the $NO_2$ vertical distribution is $\sim$ 13–40 km for both retrievals. The number of independent pieces of information, also called the degree of freedom for signal (DOFS), given by the trace of the matrix **A** (Rodgers, 2000), is about 1.2 in both cases. From this information content assessment, it can be concluded that both

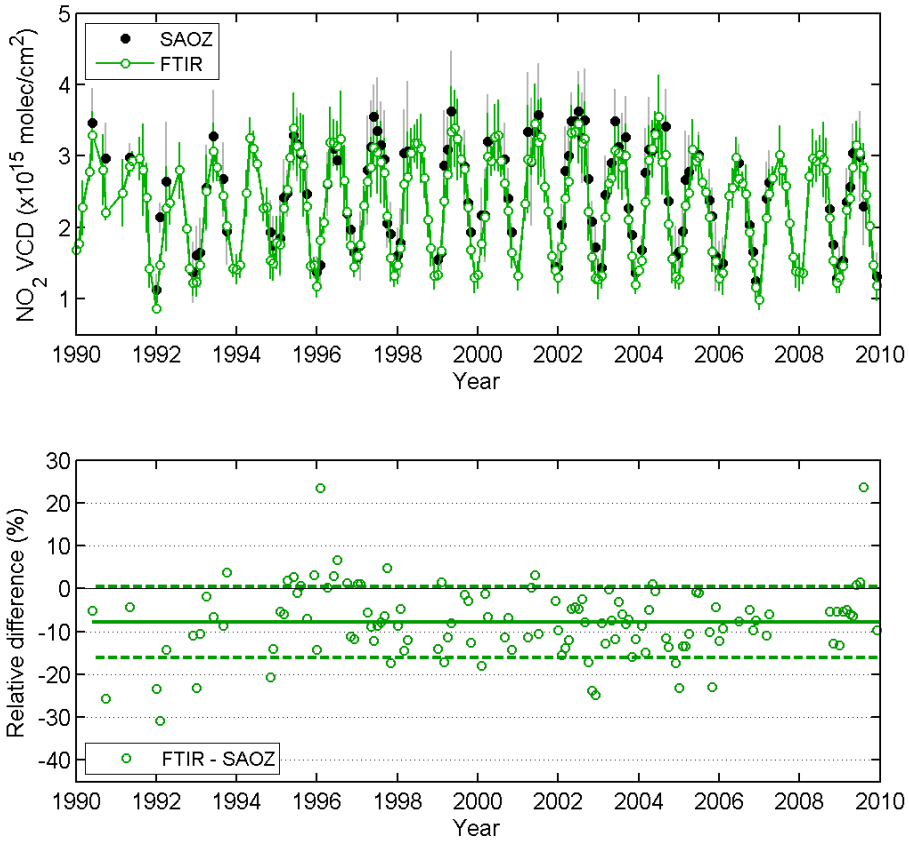


**Fig. 2.** Comparison between FTIR and SAOZ monthly mean stratospheric $NO_2$ columns at Jungfraujoch (46.5° N, 8° E) for the 1990–2009 period. The error bars correspond to the 1-sigma standard deviation (natural variability). The relative differences appear on the lower plot with solid and dashed green lines corresponding to the mean FTIR – SAOZ difference and its 1-sigma standard deviation, respectively, which is $-7.8 \pm 8.2$ %.

FTIR and SAOZ retrievals have similar vertical resolution and sensitivity to the vertical distribution of $NO_2$ and therefore retrieved $NO_2$ columns can be directly compared.

The consistency between ground-based FTIR and SAOZ data sets is evaluated by comparing the monthly mean stratospheric $NO_2$ columns for the 1990–2009 period (see Fig. 2). To ensure photochemical matching, i.e. comparison in the same photochemical conditions, the SAOZ profiles and corresponding columns, representative of twilight conditions, are converted on a daily basis to the mean FTIR measurement SZA using the PSCBOX photochemical model of the SAOZ profiling algorithm forward model (see Sect. 2.1). FTIR and SAOZ data sets are in good agreement, with FTIR measurements lower than SAOZ by $7.8 \pm 8.2$ % on average.

Combining the facts that both retrievals used similar a priori profiles and have similar sensitivity to the vertical distribution of $NO_2$, the remaining differences between FTIR and SAOZ $NO_2$ columns are consistent with the uncertainties affecting the respective spectroscopic parameters.

### 3.2 SAOZ and satellite nadir data sets comparison

SAOZ and satellite nadir (GOME, SCIAMACHY, and GOME-2) monthly mean stratospheric $NO_2$ columns are compared in Fig. 3. The retrieved SAOZ columns are photochemically converted to the satellite overpass SZA in order to perform comparisons under the same photochemical conditions. A good agreement is obtained with mean satellite minus SAOZ relative differences of $+0.9 \pm 8.8$ % (GOME), $+1.9 \pm 11.5$ % (SCIAMACHY), and $+2.3 \pm 11.6$ % (GOME-2), i.e. not significant at the 1-sigma uncertainty level. Based on these results, the composite satellite data set of monthly mean $NO_2$ columns used for trend analysis is constructed as follows: GOME data for the March 1996–June 2003 period, SCIAMACHY data for the July 2003–March 2007 period, and a merging of the SCIAMACHY and GOME-2 data for the April 2007–December 2009 period, given the fact that the biases between both satellite data sets and SAOZ observations are similar.

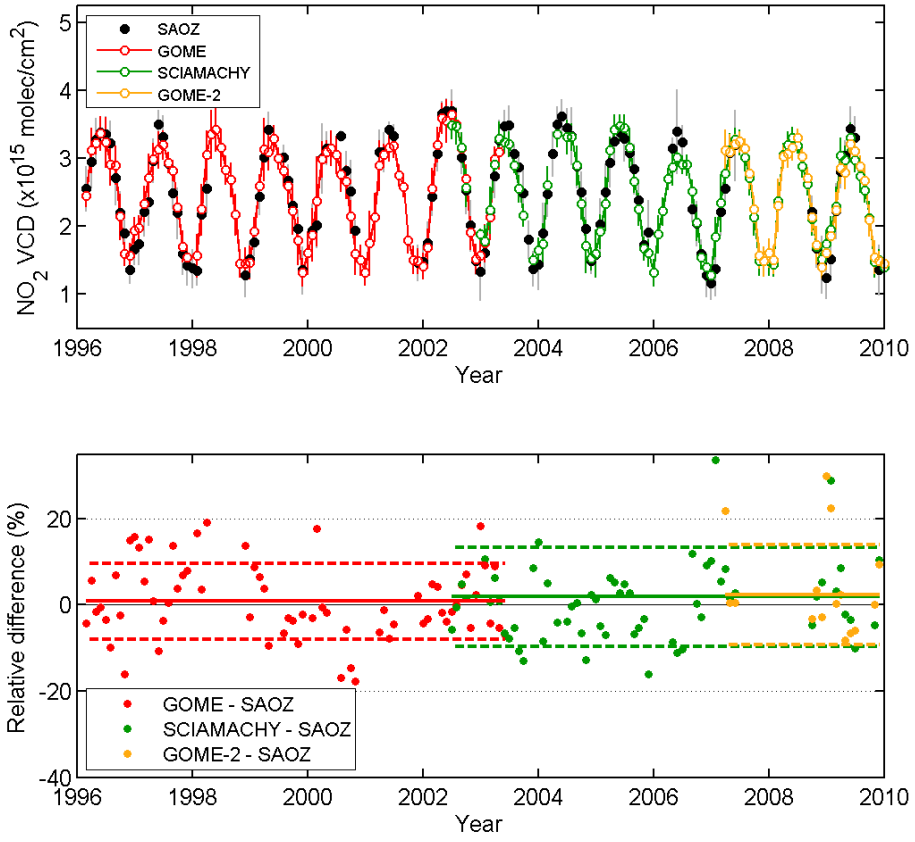


**Fig. 3.** Comparison between SAOZ and satellite nadir (GOME, SCIAMACHY, and GOME-2) monthly mean stratospheric $NO_2$ columns at Jungfraujoch (46.5° N, 8° E) for the 1996–2009 period. The error bars correspond to the 1-sigma standard deviation (natural variability). The relative differences appear on the lower plot with solid and dashed colored lines corresponding to the mean satellite – SAOZ differences and their one-sigma standard deviation, respectively, which are $+0.9 \pm 8.8$ % (GOME), $+1.9 \pm 11.5$ % (SCIAMACHY), and $+2.3 \pm 11.6$ % (GOME-2).

## 4 Trend analysis

### 4.1 Statistical model description

To extract the linear trend in the stratospheric $NO_2$ vertical column time series, a linear least squares regression model is fitted to the data to account for any extraneous variability that might affect the trend or its uncertainty. A modified version of the regression model developed by Bodeker et al. (1998) is used. It includes terms for offset, linear trend, quasi-biennial oscillation (QBO), solar activity, and aerosols effect, i.e.:

$$\begin{aligned} &m(t) = A(\mathrm{N}_A = 2) + \\ &B(\mathrm{N}_B = 2) \times t + \\ &C(\mathrm{N}_C = 2) \times \mathrm{QBO}(t) + \\ &D(\mathrm{N}_D = 0) \times \mathrm{Solar}(t) + \\ &E(\mathrm{N}_E = 1) \times \mathrm{Aerosols}(t) + \\ &U\delta \end{aligned} \tag{2}$$

where $m(t)$ is the statistically modeled monthly $NO_2$ vertical column at decimal year $t$ and $A$–$E$ are the model coefficients expanded as (for example):

$$A = A_0 + \sum_{k=1}^{\mathrm{N}_A} \left[ A_{2k-1} \sin(2\pi kt) + A_{2k} \cos(2\pi kt) \right] \tag{3}$$

to fit seasonality. The $\mathrm{N}_A$ to $\mathrm{N}_E$ coefficient values appear in Eq. (2). $U$ accounts for a possible bias between the GOME and SCIAMACHY/GOME-2 columns ($\delta$ switches from 1 to 0 in July 2003). A similar approach is applied to the SAOZ data set to account for any bias after April 1998 resulting from the installation of the new version of the SAOZ instrument.

The QBO basis function is based on the 30 and 50 hPa Singapore monthly mean zonal winds (http://www.geo.fu-berlin.de/met/ag/strat/produkte/qbo/index.html). Using these two pressure levels separately allows a covering of the altitude range of the stratospheric $NO_2$ profile and an automatic fitting of the phase of the QBO. For the solar cycle basis function, the radio-frequency

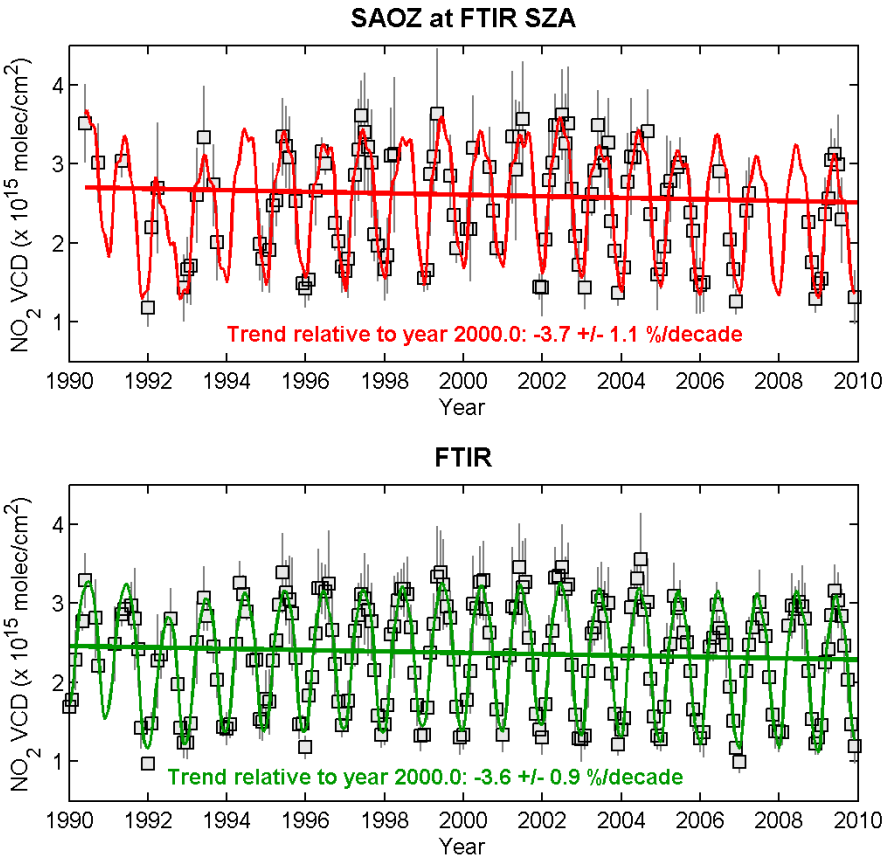


**Fig. 4.** Results of the trend analysis over the 1990–2009 period using the ground-based UV-visible SAOZ and FTIR monthly mean $NO_2$ vertical column densities (VCD; grey squares). Twilight SAOZ columns are photochemically converted to the mean SZA of the FTIR measurements. Colored lines correspond to the linear trend (thick line) and to the $NO_2$ columns recalculated using the multiple linear regression model (thin line). The error bars correspond to the 1-sigma standard deviation.

F10.7 cm solar flux (ftp://ftp.ngdc.noaa.gov/STP/SOLAR_DATA/SOLAR_RADIO/FLUX) is used. The aerosols basis function is based on the stratospheric aerosol optical depth (AOD) climatology of Vernier et al. (2011) created from SAGE II, CALIPSO, and ENVISAT/GOMOS observational data sets. The AOD time series corresponding to the 20° N–50° N latitude band was extracted for this study. This climatology includes the large changes in aerosol loading related to the Mount Pinatubo eruption as well as smaller changes due to a series of moderate volcanic eruptions, primarily at tropical latitudes, causing an increase in the stratospheric aerosol loading since 2002 (Vernier et al., 2011).

The standard deviation $\sigma_B$ on a trend $B$ can be calculated using the standard deviation $\sigma_N$ of the fit residuals (differences between modelled and observed $NO_2$ columns) and their autocorrelation coefficient $\phi$ (Weatherhead et al., 1998; van der A et al., 2006):

$$\sigma_B = \frac{\sigma_N}{n^{3/2}} \sqrt{\frac{1+\phi}{1-\phi}} \tag{4}$$

where $n$ is the length of the time series.

A test of the significance of the trend $B$ can be computed as the ratio between the trend and its standard deviation:

$$t_B = |B/\sigma_B| \tag{5}$$

A commonly applied decision rule for trend detection is that a trend is real at a 95 % confidence level when $t_B > 2$ (Weatherhead et al., 1998; Santer et al., 2000).

### 4.2 Results and discussion

Figure 4 shows the regression fits to the SAOZ and FTIR monthly mean time series and the derived trends over the period 1990–2009. The SAOZ-based trend ($-3.7 \pm 1.1$ % decade$^{-1}$; 1-sigma uncertainty) agrees with the FTIR-based trend ($-3.6 \pm 0.9$ % decade$^{-1}$). The contributions of the QBO, solar cycle, and aerosols basis functions to the signal are presented in Fig. 5. An examination of the regression fit coefficients and their respective standard deviations indicates that only the aerosols basis function makes a statistically significant contribution to the FTIR and SAOZ signals. The fact that QBO and solar cycle do not contribute

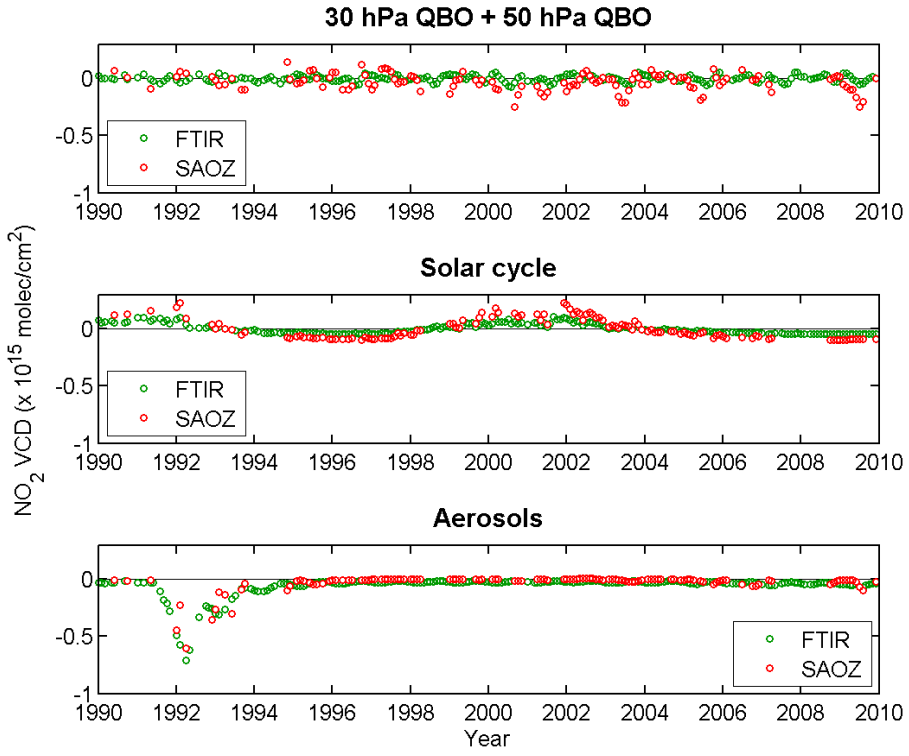


**Fig. 5.** Contributions of the QBO (upper plot), solar cycle (middle plot), and aerosols (lower plot) basis functions to the FTIR and SAOZ signals.

significantly is consistent with what Dirksen et al. (2011) found using OMI data at 50° N. We find also that the contributions of the QBO and solar cycle basis functions are larger for the SAOZ time series than for the FTIR time series. Sensitivity tests show that this results from the greater number of gaps in the SAOZ data set. The above mentioned trend values are significant at the 95 % confidence level. The uncertainty on the fit coefficients is based on the premise that the fit residuals are normally distributed. Figure 6 shows that this assumption is justified for both FTIR and SAOZ with fit residuals randomly scattered around zero and normally distributed.

A similar trend analysis is performed for the 1996–2009 period using ground-based SAOZ, FTIR, and satellite nadir data sets (see Fig. 7). For SAOZ, the trend is estimated using two data sets corresponding to the twilight $NO_2$ columns converted daily to the mean SZA of the FTIR and satellite nadir observations, respectively. Declines in $NO_2$ are seen consistently across all data sets, viz.: $-3.6 \pm 2.2$ % decade$^{-1}$ for satellites, $-2.4 \pm 1.1$ % decade$^{-1}$ for SAOZ at satellite SZA, $-4.3 \pm 1.4$ % decade$^{-1}$ for FTIR, and $-2.7 \pm 1.2$ % decade$^{-1}$ for SAOZ at FTIR SZA. It should be noted that the trend value estimated from the satellite data is not statistically significant at the 95 % confidence level. The uncertainty on the fit coefficients for the QBO, solar cycle, and aerosols basis functions indicates that none of these forcing mechanisms make a statistically significant contribution to the $NO_2$ time series measured by satellite, SAOZ, and FTIR for the 1996–2009 period.

All trend analysis results are summarized in Table 1. A good agreement is found between SAOZ, FTIR, and satellite nadir observations with a decline in the stratospheric $NO_2$ column reaching 3 % decade$^{-1}$ for both the 1990–2009 and 1996–2009 periods. This decrease is not consistent with the increase in $N_2O$ of about +2.5 % decade$^{-1}$ reported globally (WMO, 2007) and in particular from FTIR observations at the Jungfraujoch station (Angelbratt et al., 2011). Since in the $NO_y$ chemistry, $N_2O$ is the source of $NO_y$ and then $NO_y$ is subsequently partitioned into family members, opposite $NO_2$ and $N_2O$ trends suggest a change in the $NO_y$ partitioning. In the second part of this section, we discuss plausible explanations for the observed decline of $NO_2$ related or not to a $NO_y$ partitioning change.

First, $ClONO_2$ and $HNO_3$, which are two major $NO_y$ species (Brohede et al., 2008) and important chlorine and hydrogen reservoirs in the stratosphere, can be useful indicators of the abundance of $NO_2$. They are formed by the following termolecular reactions:

$$ClO + NO_2 + M \rightarrow ClONO_2 + M \quad \text{(R2)}$$

$$OH + NO_2 + M \rightarrow HNO_3 + M \quad \text{(R3)}$$

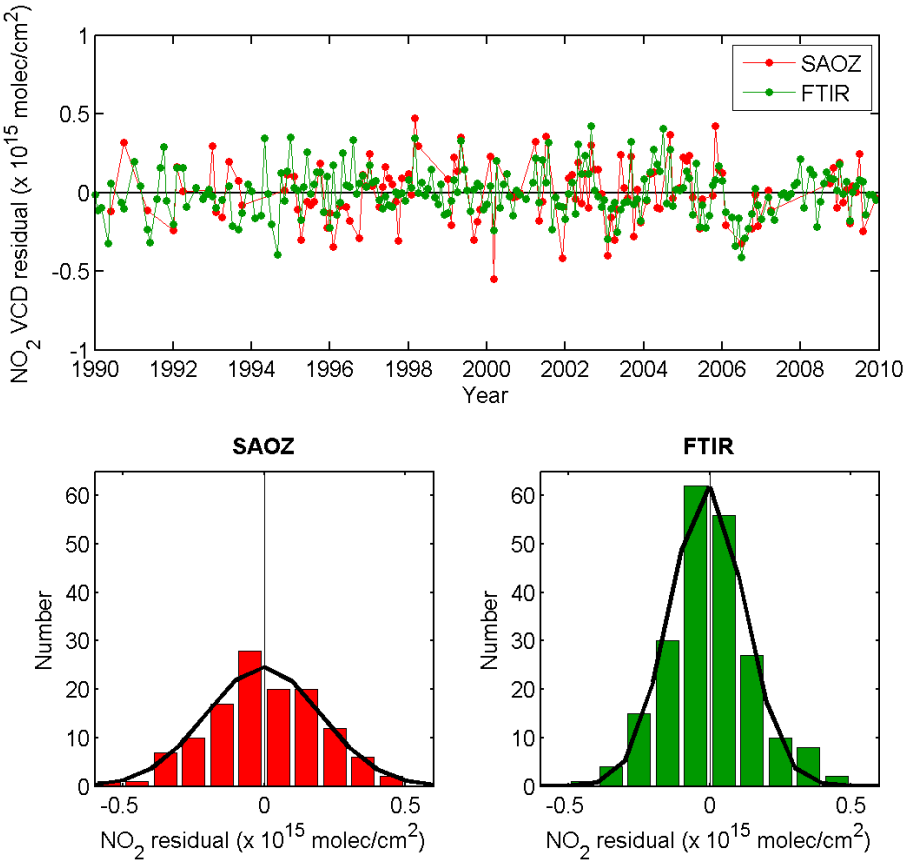


**Fig. 6.** SAOZ and FTIR fit residuals (upper plot) and their distributions (lower plots). Black lines correspond to Gaussian functions fitted on residuals distribution.

**Table 1.** Trend values in % decade$^{-1}$ derived from FTIR, SAOZ, and satellite $NO_2$ column data sets for the 1990–2009 and 1996–2009 periods. $t_B$ values appear between brackets.

| | 1990–2009 (% decade$^{-1}$) | 1996–2009 (% decade$^{-1}$) |
|---|---|---|
| FTIR | $-3.6 \pm 0.9$ (4.0) | $-4.3 \pm 1.4$ (3.1) |
| SAOZ at FTIR SZA | $-3.7 \pm 1.1$ (3.4) | $-2.7 \pm 1.2$ (2.3) |
| Satellites | – | $-3.6 \pm 2.2$ (1.6) |
| SAOZ at satellite SZA | – | $-2.4 \pm 1.1$ (2.2) |

The main loss reactions for these species are photolysis, which releases $NO_2$, as well as reactions with OH (for $HNO_3$) and dissociation on aerosols and ice particles (for $ClONO_2$). $HNO_3$ and $ClONO_2$ have been measured routinely at the Jungfraujoch station since the early 1980s using the FTIR technique (Rinsland et al., 2003b; Vigouroux et al., 2007; Wolff et al., 2008; Kohlhepp et al., 2011). This permits a trend analysis over the same time periods as was done for $NO_2$. Trend values are derived by applying the least squares regression model, described in Sect. 4.1, to the FTIR $ClONO_2$ and $HNO_3$ total column time series. Results are presented in Fig. 8. For $ClONO_2$, negative trends of $-5.8 \pm 1.0$ % decade$^{-1}$ and $-8.2 \pm 1.4$ % decade$^{-1}$ are found for the 1990–2009 and 1996–2009 periods, respectively. The latter value is more negative by about 3 % decade$^{-1}$ with respect to the trend in total tropospheric chlorine of $-6.0 \pm 0.5$ % decade$^{-1}$ observed over the same 1996–2009 period (WMO, 2011a). In the light of Reaction (R2), this larger decline of $ClONO_2$ is consistent with a decrease of stratospheric $NO_2$ of about 3 % decade$^{-1}$ as observed since 1996 from SAOZ, FTIR, and satellite nadir $NO_2$ data sets, suggesting that $NO_2$ could control the trend of $ClONO_2$ together with total chlorine. Moreover, chlorine may also play an important role in the partitioning of $NO_x$ into NO and $NO_2$ through the following reaction (Crutzen, 1979):

$$ClO + NO \rightarrow Cl + NO_2 \quad \text{(R4)}$$

Given Reaction (R4), if ClO would be decreasing, more $NO_x$ could stay in the NO form.

For $HNO_3$, positive trends of $+1.0 \pm 0.8$ % decade$^{-1}$ and $+1.9 \pm 1.2$ % decade$^{-1}$ are found for the 1990–2009 and 1996–2009 periods, respectively (see Fig. 8). Even if not statistically significant at the 95 % confidence level, this

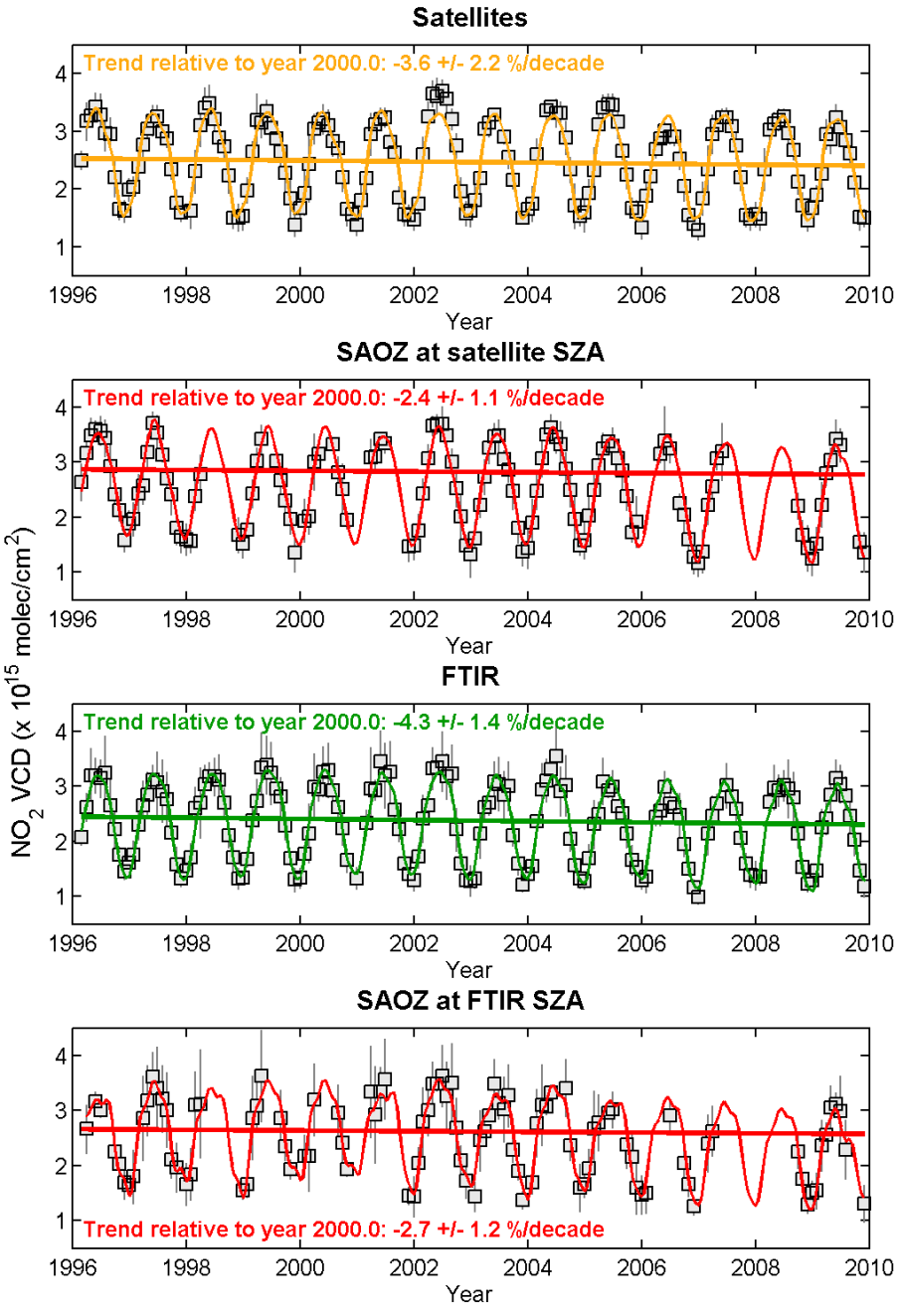


**Fig. 7.** Results of the trend analysis over the 1996–2009 period using the satellites, SAOZ, and FTIR monthly mean $NO_2$ vertical column densities (VCD; grey squares). Twilight SAOZ columns are photochemically converted to the mean SZAs of the FTIR and satellite measurements. Colored lines correspond to the linear trend (thick line) and to the $NO_2$ columns recalculated using the multiple linear regression model (thin line). The error bars correspond to 1-sigma standard deviation.

increase in $HNO_3$ is not surprising and not necessarily inconsistent with the observed decline of $NO_2$: $HNO_3$ being the most abundant $NO_y$ species in terms of column, an increase of $N_2O$ should result in a positive trend in $NO_y$ and therefore in $HNO_3$.

As discussed in the introduction, ozone can also influence the abundance of $NO_2$ in the stratosphere: a decrease in ozone leads to an increase in $NO_2$ and vice versa through Reaction (R1). We have inferred the trend in the ozone column at Jungfraujoch by applying our least squares regression model to two total ozone column data sets. The first one is based on measurements from the Dobson spectrophotometer instrument No. 101 operating at Arosa (46.8° N, 9.7° E), close to the Jungfraujoch station. The second data set

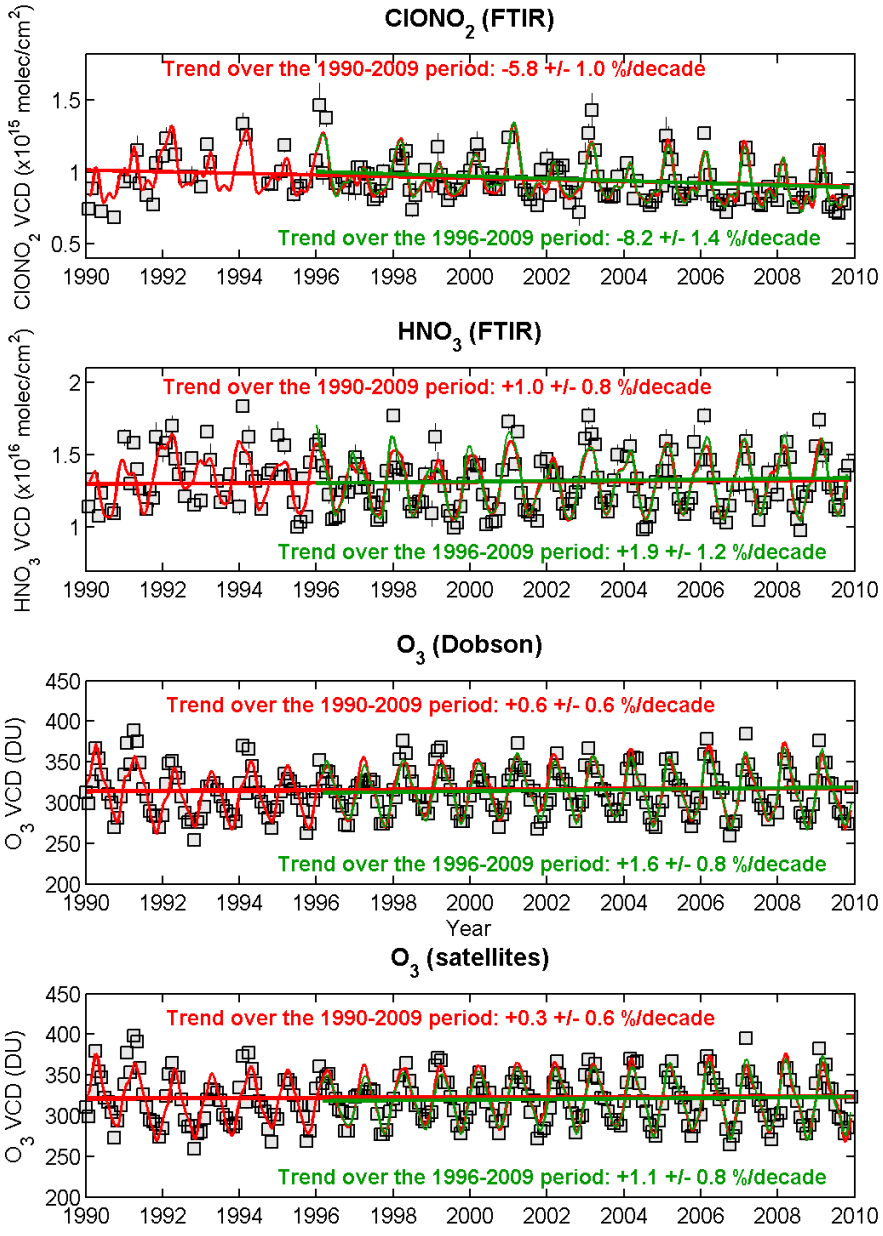


**Fig. 8.** Results of the trend analysis of the $ClONO_2$, $HNO_3$, and $O_3$ total columns measured above Jungfraujoch (above the Arosa station for Dobson measurements). Trend values are relative to year 2000.

combines satellite-based measurements from TOMS (Total Ozone Mapping Spectrometer), SBUV (Solar Backscattered Ultra-Violet), and OMI (Ozone Monitoring Instrument), and GOME instruments (Bodeker et al., 2005). A very good consistency is obtained between Dobson and satellite trend values (see Fig. 8): $+0.6 \pm 0.6\,\%\,\text{decade}^{-1}$ (Dobson) and $+0.3 \pm 0.6\,\%\,\text{decade}^{-1}$ (satellite) for 1990–2009 and $+1.6 \pm 0.8\,\%\,\text{decade}^{-1}$ (Dobson) and $+1.1 \pm 0.8\,\%\,\text{decade}^{-1}$ (satellite) for 1996–2009. It should be noted that the two latter values are also reasonably consistent with the $O_3$ trend of $+0.6 \pm 0.9\,\%\,\text{decade}^{-1}$ estimated from FTIR observations at Jungfraujoch during the 1996–2009 period (Vigouroux et al., 2008; WMO, 2011b). Given the Reaction (R1), these slight increases in ozone could at least partly contribute to the observed negative trend in $NO_2$, even if not statistically significant at the 95 % confidence level.

A change in the Dobson–Brewer circulation could also affect the evolution of stratospheric $NO_2$ (Fish et al., 2000). Cook and Roscoe (2009) recently reported a small, though not significant, increase in the stratospheric circulation of $+1.4 \pm 3.5\,\%\,\text{decade}^{-1}$ derived from SAOZ $NO_2$

observations in Antarctic summer. A strengthening speed up of the Dobson-Brewer circulation would lead to less time in the stratosphere for the conversion of $N_2O$ to reactive nitrogen, resulting in a downwards trend of the $NO_2$ vertical column.

Finally, Revell et al. (2012) recently investigated the links between $N_2O$ and $NO_x$ concentrations using chemistry-climate model simulations in order to study the past and future effectiveness of $N_2O$ in depleting stratospheric ozone. Their findings are consistent with our observations at Jungfraujoch: they showed that the $NO_2$/NO partitioning is currently changing with time to favor NO, due to stratospheric cooling, which slows the $NO + O_3 \rightarrow NO_2 + O_2$ reaction, and decreasing ClO concentrations, which slows the $NO + ClO \rightarrow NO_2 + Cl$ reaction. It should be noted that a stratospheric cooling can also decrease the amount of $NO_y$ in the stratosphere from $N_2O$ (Rosenfield and Douglass, 1998).

## 5 Summary and conclusions

We have presented consolidated time series of stratospheric $NO_2$ vertical columns at the NDACC station of Jungfraujoch retrieved from ground-based FTIR and SAOZ observations as well as from GOME, SCIAMACHY, and GOME-2 satellite nadir measurements. The time period covered by the FTIR and SAOZ observations is 1990–2009 while combining the three satellite data sets covers the 1996–2009 period. We have first performed a cross-verification of the different data sets through the comparison of FTIR and SAOZ $NO_2$ columns on one hand, and the comparison between satellite nadir and SAOZ observations on the other hand. FTIR $NO_2$ columns agree well with SAOZ columns with a bias of $-7.8 \pm 8.2$ % on average over the 1990–2009 period. A good agreement is also found between satellite nadir and SAOZ data sets with mean relative differences of $+0.9 \pm 8.8$ % (GOME), $+1.9 \pm 11.5$ % (SCIAMACHY), and $+2.3 \pm 11.6$ % (GOME-2). It should be noted that it is the first time that stratospheric $NO_2$ products from these satellite nadir instruments are validated for such an extended period.

The trend of the stratospheric $NO_2$ column has been estimated by applying a least squares regression model to the different ground-based and satellite data sets. For the analysis of trends in satellite observations, a composite data set covering the period 1996–2009 was constructed based on the comparison between the satellite and SAOZ measurements. A good consistency is found between the trends based on satellite and SAOZ measurements i.e. $-3.6 \pm 2.2$ % decade$^{-1}$ for satellite and $-2.4 \pm 1.1$ % decade$^{-1}$ for SAOZ. Similar trend values are obtained for the 1990–2009 period using SAOZ and FTIR observations ($-3.7 \pm 1.1$ % decade$^{-1}$ and $-3.6 \pm 0.9$ % decade$^{-1}$, respectively). This decline of stratospheric $NO_2$ of about 3 % decade$^{-1}$, obtained from three independent measurement techniques, provides further evidence that, at least for northern mid-latitudes, the trend in stratospheric $NO_2$ does not necessarily reflect the evolution of $N_2O$, considered as the main source of $NO_x$ in the stratosphere. The most reasonable explanation for this feature is a change in the $NO_x$ partitioning in favor of NO, due to possible stratospheric cooling (not investigated here) and the decline of chlorine content in the stratosphere, the latter being further confirmed by the observed decrease in $ClONO_2$ at the Jungfraujoch station. Since previous studies have shown that ozone can affect significantly the trend in $NO_2$, we have derived the trend of this species at Jungfraujoch using ground- and satellite-based $O_3$ measurements. The slightly positive trends obtained for the 1990–2009 and 1996–2009 periods are consistent with a decrease of $NO_2$ through the $NO_2 + O_3 \rightarrow NO_3 + O_2$ reaction. Although not investigated here, possible changes in the strength of the stratospheric circulation could also contribute to the negative trend in stratospheric $NO_2$. A strengthening of the Brewer-Dobson circulation would allow less time in the stratosphere for the conversion of $N_2O$ into reactive nitrogen, and therefore would lead to a decrease in stratospheric $NO_2$. We can also not rule out an altitude dependence of the trends, i.e. different trends for $NO_2$ and $N_2O$ since concentration profiles of both species have their maxima in the stratosphere at different altitudes (around 27–30 km and close to the tropopause, respectively).

Model-based sensitivity studies would certainly augment the interpretation of our findings, as well as similar trend analyses at other locations using FTIR, UV-visible, and satellite observations. However, these are beyond the scope of the present paper. This work also suggests that more effort should be put into consolidating the different ground-based and satellite observational data sets, which is one of the major tasks of the NDACC.

*Acknowledgements.* This research was financially supported at IASB-BIRA by the Belgian Federal Science Policy Office, Brussels (PRODEX contract A3C) and by the EU 7th Framework Programme projects SHIVA (contract 226224) and NORS (contract 284421). The University of Liège contribution was primarily supported by the Belgian Federal Science Policy Office, Brussels, through the SECPEA, A3C and AGACC-II projects. Emmanuel Mahieu is Research Associate with the F.R.S. – FNRS. We further acknowledge the contributions of the F.R.S. – FNRS and of the Fédération Wallonie-Bruxelles for funding the development of the Jungfraujoch laboratory and for supporting travel costs to the station, respectively. We thank the International Foundation High Altitude Research Stations Jungfraujoch and Gornergrat (HFSJG, Bern) for supporting the facilities needed to perform the observations. We are grateful to the many Belgian colleagues who have performed the FTIR observations used here. Work at the Eindhoven University of Technology was funded by the Netherlands Organisation for Scientific Research, NOW Vidi grant 864.09.001. GOME-2 level-1 data are provided by EUMETSAT. The SLIMCAT modeling was supported by the EU GEOmon project and NERC.

Edited by: T. Wagner

## References


Angelbratt, J., Mellqvist, J., Blumenstock, T., Borsdorff, T., Brohede, S., Duchatelet, P., Forster, F., Hase, F., Mahieu, E., Murtagh, D., Petersen, A. K., Schneider, M., Sussmann, R., and Urban, J.: A new method to detect long term trends of methane ($CH_4$) and nitrous oxide ($N_2O$) total columns measured within the NDACC ground-based high resolution solar FTIR network, Atmos. Chem. Phys., 11, 6167–6183, doi:10.5194/acp-11-6167-2011, 2011.

Bodeker, G. E., Boyd, I. S., and Matthews, W. A.: Trends and variability in vertical ozone and temperature profiles measured by ozonesondes at Lauder, New Zealand: 1986–1996, J. Geophys. Res., 103, 28661–28681, 1998.

Bodeker, G. E., Shiona, H., and Eskes, H.: Indicators of Antarctic ozone depletion, Atmos. Chem. Phys., 5, 2603–2615, doi:10.5194/acp-5-2603-2005, 2005.

Boersma, K. F., Eskes, H. J., and Brinksma, E. J.: Error analysis for tropospheric $NO_2$ retrieval from space, J. Geophys. Res., 109, D04311, doi:10.1029/2003JD003962, 2004.

Boersma, K. F., Eskes, H. J., Veefkind, J. P., Brinksma, E. J., van der A, R. J., Sneep, M., van den Oord, G. H. J., Levelt, P. F., Stammes, P., Gleason, J. F., and Bucsela, E. J.: Near-real time retrieval of tropospheric $NO_2$ from OMI, Atmos. Chem. Phys., 7, 2103–2118, doi:10.5194/acp-7-2103-2007, 2007.

Brohede, S., McLinden, C. A., Urban, J., Haley, C. S., Jonsson, A. I., and Murtagh, D.: Odin stratospheric proxy $NO_y$ measurements and climatology, Atmos. Chem. Phys., 8, 5731–5754, doi:10.5194/acp-8-5731-2008, 2008.

Chang, L., Palo, S., Hagan, M., Richter, J., Garcia, R., Riggin, D., and Frittz, D.: Structure of the migrating diurnal tide in the whole atmosphere community climate model, Adv. Space Res., 41, 1398–1407, 2008.

Chipperfield, M. P.: New version of the TOMCAT/SLIMCAT offline chemical transport model: intercomparison of stratospheric tracer experiments, Q. J. Roy. Meteor. Soc., 132, 1179–1203, doi:10.1256/qj.05.51, 2006.

Cook, P. A. and Roscoe, H. K.: Variability and trends in stratospheric $NO_2$ in Antarctic summer, and implications for stratospheric $NO_y$, Atmos. Chem. Phys., 9, 3601–3612, doi:10.5194/acp-9-3601-2009, 2009.

Crutzen, P. J.: The role of NO and $NO_2$ in the chemistry of the troposphere and stratosphere, Annual Review of Earth and Planetary Sciences, vol. 7 (A79-37176 15-42), Annual Reviews, Inc., Palo Alto, California, USA, 443–472, 1979.

Dirksen, R. J., Boersma, K. F., Eskes, H. J., Ionov, D. V., Bucsela, E. J., Levelt, P. F., and Kelder, H. M.: Evaluation of stratospheric $NO_2$ retrieved from the ozone monitoring instrument: intercomparison, diurnal cycle, and trending, J. Geophys. Res., 116, D08305, doi:10.129/2010JD014943, 2011.

Fish, D. J., Roscoe, H. K., and Johnston, P. V.: Possible causes of stratospheric $NO_2$ trend observed at Lauder, New Zealand, Geophys. Res. Lett., 27, 3313–3316, 2000.

Gil, M., Yela, M., Gunn, L. N., Richter, A., Alonso, I., Chipperfield, M. P., Cuevas, E., Iglesias, J., Navarro, M., Puentedura, O., and Rodriguez, S.: $NO_2$ climatology in the northern subtropical region: diurnal, seasonal and interannual variability, Atmos. Chem. Phys., 8, 1635–1648, doi:10.5194/acp-8-1635-2008, 2008.

Grainger, J. and Ring, J.: Anomalous Fraunhofer line profiles, Nature, 193, p. 762, 1962.

Gruzdev, A. N.: Latitudinal structure of variations and trends in stratospheric $NO_2$, Int. J. Remote Sens., 30, 4227–4246, 2009.

Hendrick, F., Barret, B., Van Roozendael, M., Boesch, H., Butz, A., De Mazière, M., Goutail, F., Hermans, C., Lambert, J.-C., Pfeilsticker, K., and Pommereau, J.-P.: Retrieval of nitrogen dioxide stratospheric profiles from ground-based zenith-sky UV-visible observations: validation of the technique through correlative comparisons, Atmos. Chem. Phys., 4, 2091–2106, doi:10.5194/acp-4-2091-2004, 2004.

Hendrick, F., Van Roozendael, M., Kylling, A., Petritoli, A., Rozanov, A., Sanghavi, S., Schofield, R., von Friedeburg, C., Wagner, T., Wittrock, F., Fonteyn, D., and De Mazière, M.: Intercomparison exercise between different radiative transfer models used for the interpretation of ground-based zenith-sky and multi-axis DOAS observations, Atmos. Chem. Phys., 6, 93–108, doi:10.5194/acp-6-93-2006, 2006.

Hendrick, F., Johnston, P. V., Kreher, K., Hermans, C., De Mazière, M., and Van Roozendael, M.: One decade trend analysis of stratospheric BrO over Harestua (60° N) and Lauder (45° S) reveals a decline, Geophys. Res. Lett., 35, L14801, doi:10.1029/2008GL034154, 2008.

Kohlhepp, R., Ruhnke, R., Chipperfield, M. P., De Mazière, M., Notholt, J., Barthlott, S., Batchelor, R. L., Blatherwick, R. D., Blumenstock, Th., Coffey, M. T., Demoulin, P., Fast, H., Feng, W., Goldman, A., Griffith, D. W. T., Hamann, K., Hannigan, J. W., Hase, F., Jones, N. B., Kagawa, A., Kaiser, I., Kasai, Y., Kirner, O., Kouker, W., Lindenmaier, R., Mahieu, E., Mittermeier, R. L., Monge-Sanz, B., Morino, I., Murata, I., Nakajima, H., Palm, M., Paton-Walsh, C., Raffalski, U., Reddmann, Th., Rettinger, M., Rinsland, C. P., Rozanov, E., Schneider, M., Senten, C., Servais, C., Sinnhuber, B.-M., Smale, D., Strong, K., Sussmann, R., Taylor, J. R., Vanhaelewyn, G., Warneke, T., Whaley, C., Wiehle, M., and Wood, S. W.: Observed and simulated time evolution of HCl, $ClONO_2$, and HF total column abundances, Atmos. Chem. Phys., 12, 3527–3556, doi:10.5194/acp-12-3527-2012, 2012.

Liley, J. B., Johnston, P. V., McKenzie, R. L., Thomas, A. J., and Boyd, I. S.: Stratospheric $NO_2$ variations from a long time series at Lauder, New Zealand, J. Geophys. Res., 105, 11633–11640, 2000.

McLinden, C. A., Olsen, S. C., and Prather, M. J.: Understanding trends in stratospheric $NO_y$ and $NO_2$, J. Geophys. Res., 106, 27787–27793, 2001.

Platt, U. and Stuz, J.: Differential Optical Absorption Spectroscopy (DOAS), Principles and Applications, ISBN 978-3-540-21193-8, Springer, Berlin, Heidelberg, Germany, 2008.

Pommereau, J.-P. and Goutail, F.: $O_3$ and $NO_2$ ground-based measurements by visible spectrometry during arctic winter and spring 1988, Geophys. Res. Lett., 15, 891–894, 1988.

Pougatchev, N. S. and Rinsland, C. P.: Spectroscopic study of the seasonal variation of carbon monoxide vertical distribution above Kitt Peak, J. Geophys. Res., 100, 1409–1416, 1995.

Revell, L. E., Bodeker, G. E., Smale, D., Lehmann, R., Huck, P. E., Williamson, B. E., Rozanov, E., and Struthers, H.: The effectiveness of $N_2O$ in depleting stratospheric ozone, Geophys. Res.

Lett., 39, L15806, doi:10.1029/2012GL052143, 2012.

Rinsland, C. P., Weisenstein, D. K., Ko, M. K. W., Scott, C. J., Chiou, L. S., Mahieu, E., Zander, R., and Demoulin, P.: Post Mount Pinatubo eruption ground-based stratospheric column measurements of $HNO_3$, NO, and $NO_2$ and their comparison with model calculation, J. Geophys. Res., 108, 4437, doi:10.1029/2002JD002965, 2003a.

Rinsland, C. P., Mahieu, E., Zander, R., Jones, N. B., Chipperfield, M. P., Goldman, A., Anderson, J., Russell III, J. M., Demoulin, P., Notholt, J., Toon, G. C., Blavier, J.-F., Sen, B., Sussmann, R., Wood, S. W., Meier, A., Griffith, D. W. T., Chiou, L. S., Murcray, F. J., Stephen, T. M., Hase, F., Mikuteit, S., Schulz, A., and Blumenstock, T.: Long-term trends of inorganic chlorine from ground-based infrared solar spectra: past increases and evidence for stabilization, J. Geophys. Res., 108, 4252, doi:10.1029/2002JD003001, 2003b.

Rosenfield, J. E. and Douglass, A. R.: Doubled $CO_2$ effects on $NO_y$ in a coupled 2-D model, Geophys. Res. Lett., 25, 4381–4384, 1998.

Rothman, L. S., Jacquemart, D., Barbe, A., Chris Benner, D. Birk, M., Brown, L. R., Carleer, M. R., Chackerian Jr., C., Chance, K., Coudert, L. H., Dana, V., Devi, V. M., Gamache, R. R., Goldman, A., Jucks, K. W., Maki, A. G., Massie, S. T., Orphal, J., Perrin, A., Rinsland, C. P., Smith, M. A. H., Tennyson, J., Tolchenov, Toth, R. A., Vander Auwera, J., Varanasi, P., and Wagner, G.: The HITRAN 2004 molecular spectroscopic database, J. Quant. Spectrosc. Ra., 96, 139–204, 2005.

Santer, B. D., Wigley, T. M. L., Boyle, J. S., Gaffen, D. J., Hnilo, J. J., Nychka, D., Parker, D. E., and Taylor, K. E.: Statistical significance of trends and trend differences in layer-average atmospheric temperature time series, J. Geophys. Res., 105, 7337–7356, 2000.

Shettle, E. P.: Models of aerosols, clouds, and precipitation for atmospheric propagation studies, in: NATO AGARD Conference Proceedings No. 454: atmospheric propagation in the UV, visible, IR and mm-region and related system aspects, NATO (North Atlantic Treaty Organisation), Neuilly sur Seine, France, 1989.

Solomon, S.: Stratospheric ozone depletion: a review of concepts and history, Rev. Geophys., 37, 275–316, 1999.

Vandaele, A. C., Hermans, C., Simon, P. C., Carleer, M., Colin, R., Fally, S., Mérienne, M.-F., Jenouvrier, A., and Coquart, B.: Measurements of the $NO_2$ absorption cross section from 42 000 $cm^{-1}$ to 10000 $cm^{-1}$ (238–1000 nm) at 220 K and 294 K, J. Quant. Spectrosc. Ra., 59, 171–184, 1998.

van der A, R. J., Peters, D. H. M. U., Heskes, H., Boersma, K. F., Van Roozendael, M., De Smedt, I., and Kelder, H.: Detection of the trend and seasonal variation in tropospheric $NO_2$ over China, J. Geophys. Res., 111, D12317, doi:10.1029/2005JD006594, 2006.

Van Roozendael, M., De Mazière, M., and Simon, P. C.: Ground-based visible measurements at the Jungfraujoch station since 1990, J. Quant. Spectrosc. Ra., 52, 231–240, 1994.

Vernier, J.-P., Thomason, L. W., Pommereau, J.-P., Bourassa, A., Pelon, J., Garnier, A., Hauchecorne, A., Blanot, L., Trepte, C., Degenstein, D., and Vargas, F.: Major influence of tropical volcanic eruptions on the stratospheric aerosol layer during the last decade, Geophys. Res. Lett., 38, L12807, doi:10.129/2011GL047563, 2011.

Vigouroux, C., De Mazière, M., Errera, Q., Chabrillat, S., Mahieu, E., Duchatelet, P., Wood, S., Smale, D., Mikuteit, S., Blumenstock, T., Hase, F., and Jones, N.: Comparisons between ground-based FTIR and MIPAS $N_2O$ and $HNO_3$ profiles before and after assimilation in BASCOE, Atmos. Chem. Phys., 7, 377–396, doi:10.5194/acp-7-377-2007, 2007.

Vigouroux, C., De Mazière, M., Demoulin, P., Servais, C., Hase, F., Blumenstock, T., Kramer, I., Schneider, M., Mellqvist, J., Strandberg, A., Velazco, V., Notholt, J., Sussmann, R., Stremme, W., Rockmann, A., Gardiner, T., Coleman, M., and Woods, P.: Evaluation of tropospheric and stratospheric ozone trends over Western Europe from ground-based FTIR network observations, Atmos. Chem. Phys., 8, 6865–6886, doi:10.5194/acp-8-6865-2008, 2008.

Weatherhead, E. C., Reinsel, G. C., Tiao, G. C., Meng, X., Choi, D., Cheang, W., Keller, T., DeLuisi, J., Wuebbles, D. J., Kerr, J. B., Miller, A. J., Oltmans, S. J., and Frederick, J. E.: Factors affecting the detection of trends: statistical considerations and applications to environmental data, J. Geophys. Res., 103, 17149–17161, 1998.

WMO (World Meteorological Organization): Scientific Assessment of Ozone depletion: 2006 (chapt. 4), Global Ozone Research and Monitoring Project, Report 50, World Meteorological Organization, Geneva, Switzerland, 2007.

WMO (World Meteorological Organization): Scientific Assessment of Ozone depletion: 2010 (chapt. 1), Global Ozone Research and Monitoring Project, Report 52, World Meteorological Organization, Geneva, Switzerland, 2011a.

WMO (World Meteorological Organization): Scientific Assessment of Ozone depletion: 2010 (chapt. 2), Global Ozone Research and Monitoring Project, Report 52, World Meteorological Organization, Geneva, Switzerland, 2011b.

Wolff, M. A., Kerzenmacher, T., Strong, K., Walker, K. A., Toohey, M., Dupuy, E., Bernath, P. F., Boone, C. D., Brohede, S., Catoire, V., von Clarmann, T., Coffey, M., Daffer, W. H., De Mazière, M., Duchatelet, P., Glatthor, N., Griffith, D. W. T., Hannigan, J., Hase, F., Höpfner, M., Huret, N., Jones, N., Jucks, K., Kagawa, A., Kasai, Y., Kramer, I., Küllmann, H., Kuttippurath, J., Mahieu, E., Manney, G., McElroy, C. T., McLinden, C., Mébarki, Y., Mikuteit, S., Murtagh, D., Piccolo, C., Raspollini, P., Ridolfi, M., Ruhnke, R., Santee, M., Senten, C., Smale, D., Tétard, C., Urban, J., and Wood, S.: Validation of $HNO_3$, $ClONO_2$, and $N_2O_5$ from the Atmospheric Chemistry Experiment Fourier Transform Spectrometer (ACE-FTS), Atmos. Chem. Phys., 8, 3529–3562, doi:10.5194/acp-8-3529-2008, 2008.

Zander, R., Mahieu, E., Demoulin, P., Duchatelet, P., Roland, G., Servais, C., De Mazière, M., Reimann, S., and Rinsland, C. P.: Our changing atmosphere: evidence based on long-term infrared solar observations at the Jungfraujoch since 1950, Sci. Total Environ., 391, 184–195 doi:10.1016/j.scitotenv.2007.10.018, 2008.